NEUROSCIENCE

Early peripheral activity alters nascent subplate circuits in the auditory cortex

Xiangying Meng[1,2]*, Didhiti Mukherjee[1,2]*, Joseph P. Y. Kao[3], Patrick O. Kanold[1,2,4]†

Cortical function can be shaped by sensory experience during a critical period. The onset of the critical period is thought to coincide with the onset of thalamocortical transmission to the thalamo-recipient layer 4 (L4). In early development, subplate neurons (SPNs), and not L4 neurons, are the first targets of thalamic afferents. SPNs are transiently involved in early development and are largely eliminated during development. Activation of L4 by thalamic afferents coincides with the opening of ear canal (~P11 in mice) and precedes the later critical period. Here, we show in mice that abolishing peripheral function or presenting sound stimuli even before P11 leads to bidirectionally altered functional connectivity of SPNs in auditory cortex. Thus, early sensory experience can sculpt subplate circuits before thalamocortical circuits to L4 are mature. Our results show that peripheral activity shapes cortical circuits in a sequential manner and from earlier ages than has been appreciated.

INTRODUCTION

Sensory experience profoundly shapes the developing brain. In adult sensory cortex, thalamocortical (TC) axons target layer 4 (L4) and the effects of early sensory experience in all sensory systems have been investigated in L4 neurons and subsequent processing stages (*1*–*7*). Initially, developing TC axons do not innervate L4 but instead excite earlier-born subplate neurons (SPNs) before growing into L4 (Fig. 1A) (*8*, *9*). In humans, SPNs mature within the second trimester (*8*), during which fetal responses to sound emerge (*10*, *11*). In mouse, this developmental period lasts to around ear opening at postnatal (P) day 11 (*1*, *8*). SPNs receive intracortical inputs, associate ascending and intracortical activity (*9*, *12*, *13*), project to L4 (*14*, *15*), and thus can influence the development of L4 (*8*). SPNs are largely eliminated during development (*16*–*20*), but early removal of SPNs prevents development of both TC and intracortical circuits, indicating that SPNs are essential for cortical development (*8*, *9*, *21*–*23*). SPN circuits can be altered because of environmental insults (*24*, *25*), and SPNs have been implicated in neurodevelopmental disorders (*24*, *26*). Because SPNs respond to sounds before TC activation of L4 (~P21 in ferrets, equivalent to ~P6 in mice) (*27*), we hypothesized that early peripheral spontaneous (*28*–*30*) and sound-generated activity might influence early-maturing SPN circuits in auditory cortex (ACtx) before the maturation of TC transmission to L4 (*1*) and that, as such, sensory stimuli might have an earlier effect on cortical circuits than previously appreciated.

RESULTS

In rodents, spontaneous activity originating in the cochlea (*28*) is present in ACtx at P7 (*29*). Sound-evoked auditory brainstem responses are present in rodents at ~P7/P8 before ear canal opening (*31*), and sounds can activate ACtx neurons in mouse before P10 (*32*).

To confirm the presence of both spontaneous and sound-evoked activity in ACtx before ear opening, we performed in vivo widefield imaging in awake mice expressing the Ca^{2+} indicator GCaMP6s in excitatory neurons (Fig. 1, A and B) (*33*). Widefield imaging ($n = 6$, P8 to P9; $n = 5$, P13 to P15) revealed spontaneous and sound-evoked activity (Fig. 1C). Presenting 80-dB tones significantly increased mean fluorescence amplitude at both ages (Fig. 1D). Neural activity is composed of low (L)– and high (H)–synchronization events (Fig. 1E), which are distinguished by size and, in visual cortex, reflect peripheral and central sources, respectively (*34*). The inter-event intervals showed that the frequency of H-events decreased with development, whereas that of L-events increased ($P < 0.001$; Fig. 1F), suggesting more peripheral inputs after ear opening. The peak amplitude of spontaneous and sound-evoked H- and L-events decreased with development ($P < 0.001$; Fig. 1F, right), consistent with single-cell data (*32*). Cochlear removal abolished sound-evoked events, reduced the amplitude of spontaneous L-events, and increased the amplitude of spontaneous H-events (fig. S1, A to C), consistent with L-events reflecting peripheral sources. Thus, both spontaneous and sound-evoked responses are present in mouse ACtx before ear canal opening.

Connections to SPNs in deaf mice are altered at P6 to P9

Because sound-evoked activity was present in ACtx before ear opening, we next investigated whether manipulation of peripheral activity could shape the connectivity of SPNs before natural ear canal opening. We investigated the functional connectivity of SPNs in mice deficient in transmembrane channel–like 1 and 2 [TMC1/2-DKO (double knockout)], which is required for cochlear mechanotransduction (*35*, *36*). Mice deficient in both TMC1 and TMC2 never develop mechanotransduction in the cochlea and are thus profoundly deaf (*35*–*37*). In vivo widefield imaging in awake TMC1/2-DKO mice showed a lack of tone-evoked cortical activity (fig. S1, D to F).

To evaluate the functional intracortical connectivity to SPNs in these deaf mice, we used laser scanning photostimulation (LSPS) combined with whole-cell patch clamp recordings (*12*, *13*) from different cortical layers in TC slices of ACtx (Fig. 2, A and B). In these slices, the rostro-caudal tonotopic axis is preserved. With LSPS, presynaptic neurons are activated optically (Fig. 2B), allowing assessment of the functional spatial connection pattern of SPNs. We first

[1]Department of Biomedical Engineering, Johns Hopkins University, Baltimore, MD 21205, USA. [2]Department of Biology, University of Maryland, College Park, MD 20742, USA. [3]Center for Biomedical Engineering and Technology and Department of Physiology, University of Maryland School of Medicine, Baltimore, MD 21201, USA. [4]Kavli Neuroscience Discovery Institute, Johns Hopkins University, Baltimore, MD 21205, USA.
*These authors contributed equally to this work.
†Corresponding author. Email: pkanold@jhu.edu

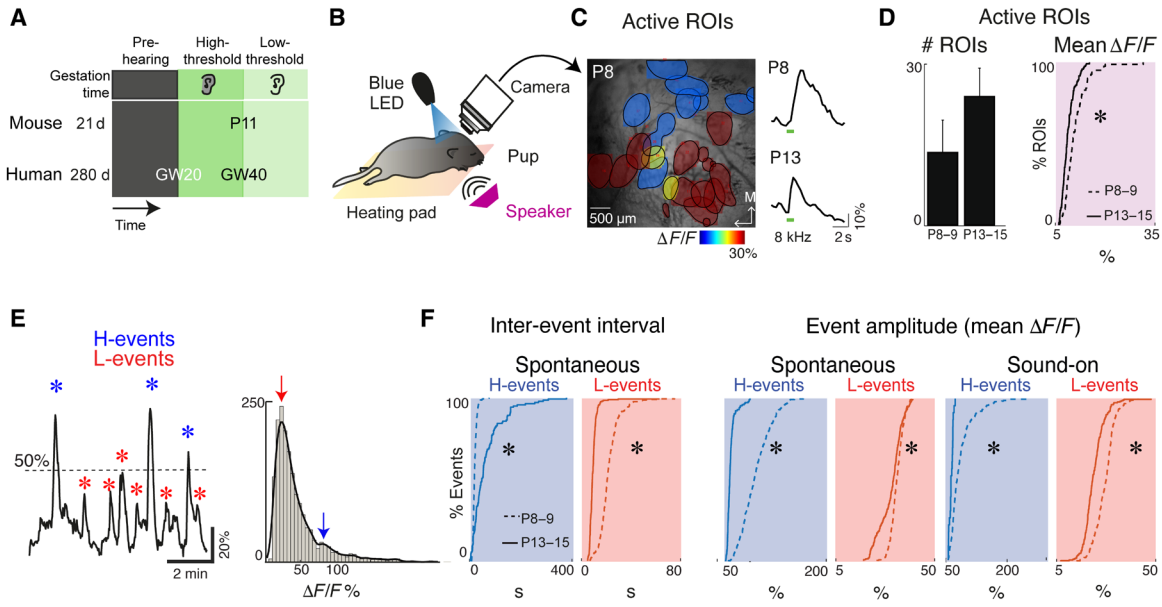

Fig. 1. Mouse ACtx shows spontaneous and sound-evoked activity before ear opening. (**A**) Timeline of cortical development in various species. Mouse ears open at ~P10. (**B**) Experimental setup and fluorescence image of activity. (**C**) Left: Filled areas indicate active ROIs that showed responses to sound. Colors indicate mean Δ*F*/*F* of active ROIs in a 2-s window after tone onset. Right: Exemplar fluorescence time courses of two single active ROIs during 8-kHz tone presentation. (**D**) Left: Bar graphs showing numbers of active ROIs at both ages (means ± SD; P8 to P9: 13.67 ± 7.5, P13 to P15: 24.2 ± 5.4; $P > 0.05$). Right: CDFs (cumulative distribution functions) showing that mean Δ*F*/*F* of active ROIs in a 2-s window after tone onset is higher at P8 to P9 (dashed, median: 10.2%) than that at P13 to P15 (solid, median: 8.5%; $P < 0.001$). (**E**) Spontaneous activity shows low (L)– and high (H)–synchronization events. (**F**) Inter-event interval and peak amplitudes of L- and H-events of spontaneous and sound-evoked activity over all the repeats and sound stimuli for all ROIs at P8 to P9 (dashed) and P13 to P15 (solid). Inter-event interval of H-events is longer and that of L-events is shorter at P13 to P15 than those at P8 to P9, respectively (H-event medians, P8 to P9: 18.7 s, P13 to P15: 44.5 s; L-event medians, P8 to P9: 20.6 s, P13 to P15: 8.9 s; $P < 0.001$ for both). The peak amplitudes of both H and L spontaneous events are higher at P8 to P9 (H-event medians, P8 to P9: 92.4%, P13 to P15: 56%; L-event medians, P8 to P9: 32.7%, P13 to P15: 31.2%; $P < 0.001$ for both), and those after sound onset are also higher at P8 to P9 (H-event medians, P8 to P9: 72.8%, P13 to P15: 57%; L-event medians, P8 to P9: 27.5%, P13 to P15: 21.4%; $P < 0.001$ for both).

ensured that LSPS caused similar activation of targeted cells in wild-type (WT) ($TMC1^{+/+}/2^{+/+}$) and TMC1/2-DKO mice. Cell-attached patch clamp recordings from WT mice raised under ambient colony conditions (control) and TMC1/2-DKO showed that photostimulation evoked action potentials in cells with equal spatial resolution (fig. S2). Moreover, the numbers of action potentials generated by the stimulation pulse were similar between groups, indicating that the loss of TMC1/2 did not alter the sensitivity of cortical neurons to photoreleased glutamate (fig. S2). Thus, these experiments show that LSPS activates neurons in both groups equally and hence allows the comparison of circuits in the two groups.

We next measured the spatial pattern of excitatory inputs to SPNs in the two groups of mice at the end of the first postnatal week (PNW) (P6 to P9) ($N = 65$ control and $N = 33$ TMC1/2-DKO). For each SPN, we stimulated 900 to 1000 presynaptic locations within the slice and measured the amplitude of evoked excitatory postsynaptic currents (eEPSCs) and inhibitory PSCs (eIPSCs) from each stimulus location by holding the SPN at −70 mV (E_{GABA}) or 0 mV ($E_{Glutamate}$), respectively (Fig. 2B). To visualize the average connectivity of the recorded neurons, we derived spatial connection maps by plotting the eEPSC or eIPSC charge at each stimulus location (Fig. 2C). We aligned the individual connection maps to the position of SPN somata and calculated the fraction of cells receiving inputs from a particular location (Fig. 2D), which yields a map of the spatial connection probability for excitatory and inhibitory connections (Fig. 2, E and G). A high connection probability (e.g., red pseudocolor in the map) indicates that many cells in our sample received input from this particular location. Qualitatively, these maps showed higher connection probabilities in TMC1/2-DKO in areas of L5/6 and subplate as well as a larger area showing high connection probability. These observations suggested that SPNs from TMC1/2-DKO mice had an increased probability to receive inputs from lower cortical layers than SPNs from control animals (Fig. 2, E and G).

We next quantified the differences in intracortical circuits impinging on SPNs in TMC1/2-DKO and control. For each individual SPN, we measured the area from which inputs originated in each layer reflecting sublaminar rearrangement, the amplitude (charge) of inputs from each layer, and the spatial range of inputs along the tonotopic (rostro-caudal) axis within each layer reflecting the intralaminar integration. SPNs from TMC1/2-DKO mice showed larger areas for inputs from L5/6 and subplate. Moreover, the intralaminar integration of inputs from L5/6 was increased. These results indicate that SPNs from TMC1/2-DKO mice received excitatory inputs from more and more widely spaced locations in L5/6 and from within subplate than SPNs from control animals, indicating hyperconnectivity (Fig. 2F). In addition, the strength of eEPSCs arising from L4 and subplate was increased in TMC1/2-DKO SPNs (Fig. 2F). SPNs from TMC1/2-DKO also showed an increased amount of inhibitory connections from within subplate and an increased amplitude of connections from L4 (Fig. 2H). To test whether changes in laminar inputs in excitatory inputs and inhibitory inputs are of similar magnitude, we calculated the excitation/inhibition (E/I) balance index for each layer. This index shows the relative amount of excitatory versus inhibitory inputs, for example, when calculated based on area

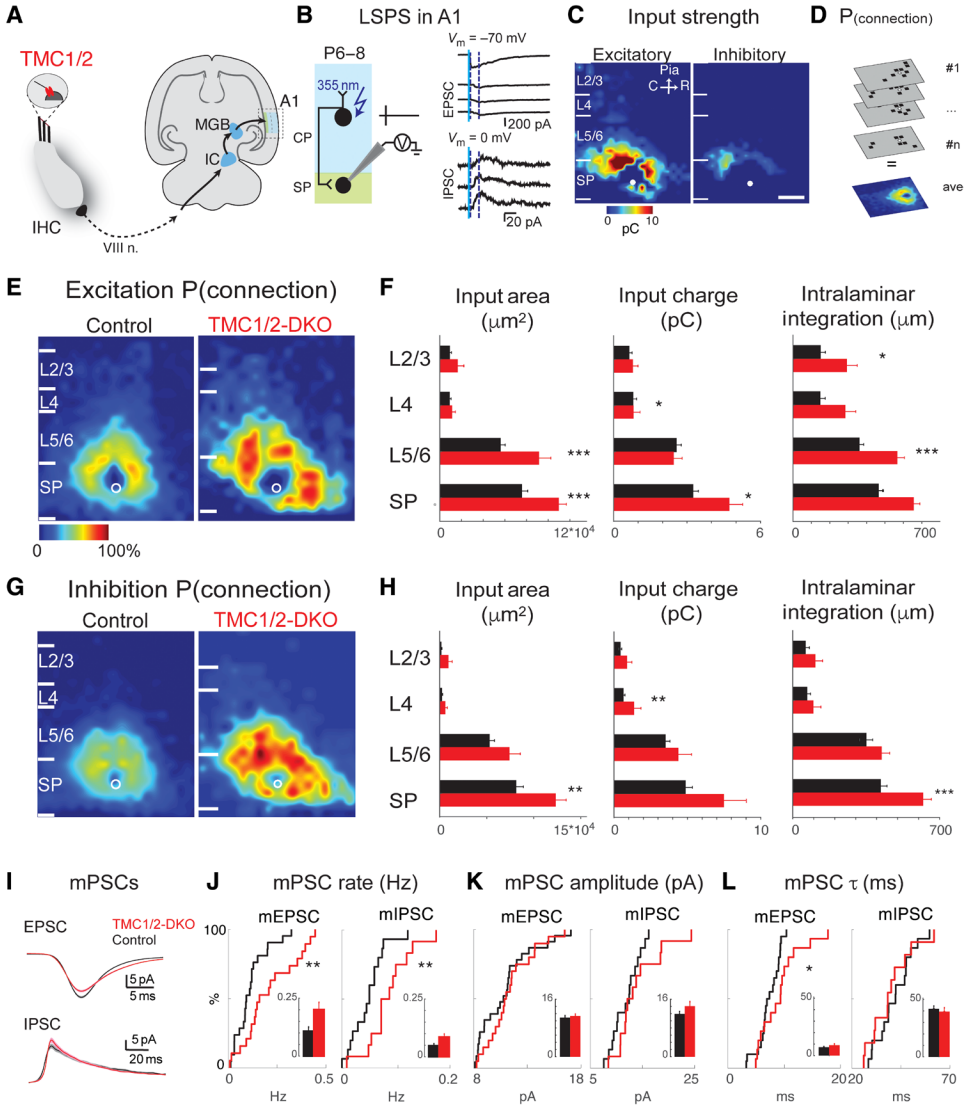

Fig. 2. Excitatory circuits to SPNs at end of first PNW are expanded in deaf mice. (**A**) Schematic of hair cell showing location of TMCs on tip link of cochlear inner hair cell (IHC). Hair cell activity is transmitted to the primary ACtx (A1) via auditory nerve (VIII n.), brainstem nuclei, inferior colliculus (IC), and medial geniculate body (MGB). (**B**) Experimental design. Neurons are activated by laser photolysis (355 nm) of caged glutamate. If stimulated cells are connected to recorded SPN, evoked excitatory or inhibitory postsynaptic currents (eEPSCs or eIPSCs) are seen. Right: Exemplar eEPSCs and eIPSCs from different stimulus locations. (**C**) Exemplar eEPSC and eIPSC charge maps. Layer borders indicated by white bars. Scale bar, 100 μm. (**D**) Individual event maps are aligned to SPN somata and averaged to derive connection probability map. (**E**) Spatial connection probability map for eEPSCs. (**F**) Left: Total area in each layer from which eEPSCs can be evoked. Middle: Mean eEPSC charge. Right: Rostro-caudal extent of laminar inputs along the tonotopic axis. (**G**) Spatial connection probability map for eIPSCs. (**H**) Same as (F) for eIPSCs. (**I** to **L**) mPSC recordings. (I) mEPSC and mIPSC traces in SPNs from TMC1/2-DKO and control. Solid lines represent the mean mPSC, and shadows represent the SEM. (J to L) mPSC rate, amplitude, and decay time constants. Bar graphs show means. For all plots, *$P < 0.05$, **$P < 0.01$, and ***$P < 0.001$. See fig. S9 and tables S1 and S2.

whether a larger area contributes excitatory versus inhibitory inputs. Because we cannot measure excitatory inputs close to the soma, we did not calculate this index for these locations. Calculating the E/I balance index for each layer showed no differences between control and TMC1/2-DKO, indicating that the excitatory and inhibitory circuit changes in TMC1/2-DKO were of equal magnitude (fig. S3A).

So far, our results suggest that SPN from TMC1/2-DKO received more excitatory and inhibitory inputs. To independently validate our results, we recorded miniature EPSCs (mEPSCs) and IPSCs (mIPSCs) in SPNs from a separate cohort of animals. We find that mEPSCs and mIPSCs were more frequent in SPNs from TMC1/2-DKO than control (N = 24 WT and N = 20 TMC1/2-DKO; $P < 0.05$), indicating that SPNs in TMC1/2-DKO received more but similarly sized synaptic inputs (Fig. 2, I to K). mEPSCs in TMC1/2-DKO also showed longer decay kinetics (Fig. 2L), consistent with the increased charge in the LSPS data (Fig. 2, F and H). Similar to the LSPS results, the mPSC changes were balanced (fig. S3B).

The connection probability measures, at each location, the average fraction of cells that receive inputs from a particular location. Thus, an increased connection probability (Fig. 2, E and G) can arise from cells showing more stereotyped connections (*32*). Individual cells can vary in their inputs, and functional circuit diversity emerges

with age (*32*). We thus investigated the spatial diversity of the circuits impinging on SPNs by calculating the variability of connections from each spatial location. For each location, we calculated the Fano factor (σ^2/mean) from the PSCs evoked in each neuron from that stimulus location. TMC1/2-DKO showed lower Fano factor in their excitatory and inhibitory inputs from L5/6 and subplate, suggesting decreased diversity in these inputs (Fig. 3, A and B). We validated this decreased circuit diversity by calculating the similarity (spatial correlation) between connection maps within each population (*32*). Cells from TMC1/2-DKO mice showed increased circuit similarity of their excitatory and inhibitory connections, consistent with the decreased Fano factor (Fig. 3C). Thus, the lack of early peripheral activity resulted in decreased circuit diversity in SPNs. Together, these results suggest that decreased peripheral activity (spontaneous and sound-evoked) alters the development of the earliest cortical circuits to SPNs.

Early sound experience alters connections to SPN

Because removal of sound transduction alters SPN circuits, this implies that SPN circuits can be modulated by early sound experience.

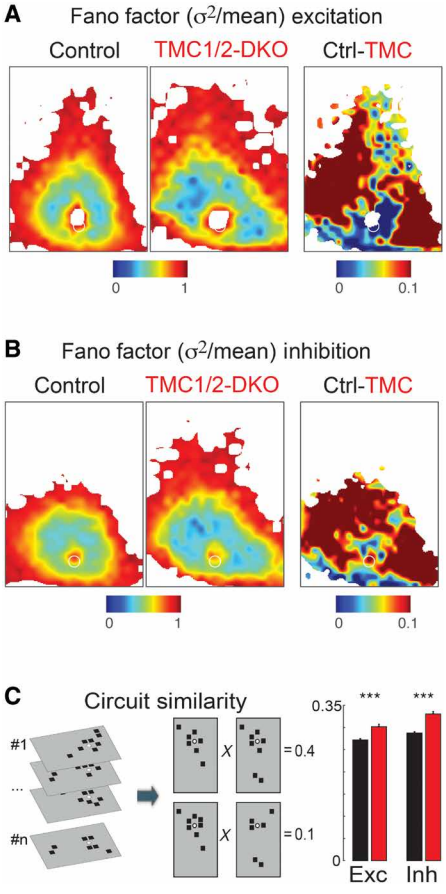

Fig. 3. Excitatory circuits to SPNs at end of first PNW are more similar in deaf mice. (**A**) Fano factor of excitatory maps and difference in Fano factor between WT and TMC1/2-DKO groups. Fano factor maps show decreased variability in TMC1/2-DKO. White color represents areas where the probability of the connections is <10%, where a Fano factor is not computed. (**B**) Fano factor of inhibitory connections. (**C**) Circuit similarity (correlation) between input maps in each group shows increased population correlations in TMC1/2-DKO. ***$P < 0.001$.

To directly test whether neonatal sound experience has the potential to sculpt SPN circuits, we raised mice from P2 in the presence of tonal stimuli (4 to 32 kHz, 80 dB) in a sound attenuation chamber (>20 dB above 1 kHz) (*38*). As a control, we raised animals in the sound attenuation chamber without tonal stimuli (no sound). Because the ear canals are closed before P11, the tone level was <20 dB above threshold. Because immature synapses and neurons adapt rapidly (*27*), we presented tones at 30-s intervals and randomized their frequencies. We then analyzed the connection pattern of SPNs ($N = 21$, no sound; $N = 32$, tone-reared) at the end of the first PNW (P6 to P9) using LSPS. The spatial connection probability showed a decrease in medium distance connections (fig. S4A) but no overall decrease in inputs (Fig. 4A). After tone rearing, SPNs showed increased amplitude of excitatory and inhibitory L5/6 inputs (Fig. 4, A and B). Calculating the E/I balance index showed that early tone exposure decreased the E/I balance index for inputs arising within subplate (fig. S5). Analyzing the circuit diversity revealed an increased Fano factor and decreased circuit correlations, indicating increased circuit variability for both excitatory (Fig. 4, A and C) and inhibitory inputs (Fig. 4, B and D). These results indicate that very early exposure to tones can alter cortical circuits and, in particular, circuit diversity.

Mice are exposed to a variety of ambient sounds in the mouse colony (*39*). We thus next asked whether these ambient sounds [in our colony average <45 dB (*40*)] are sufficient to induce circuit changes in SPNs. We compared SPNs from P6 to P8 mice ($N = 65$; Fig. 2) raised with ambient colony sounds with SPNs from mice raised without external ambient sounds ($N = 21$; Fig. 4). This comparison showed that SPNs from animals raised without external sounds exhibit hyperconnectivity of excitatory and inhibitory connections (Fig. 5, A and B), mirroring the effect of deafness. Moreover, SPNs under no-sound conditions showed higher circuit similarity (Fig. 5C). The E/I balance indices were similar (fig. S6). We confirmed these observations by recording mEPSC and mIPSC in a separate cohort of mice (Fig. 5D). SPNs from mice in no-sound conditions showed higher mEPSCs rates than SPNs from ambient conditions ($N = 22$ and 13 cells, respectively; $P < 0.05$), suggesting an increased number of inputs (Fig. 5E). These results are consistent with the hyperconnectivity observed with LSPS. Thus, ambient colony sounds are sufficient to induce changes in SPN circuits.

We next asked whether longer sound exposures would result in stronger effects, especially because the natural opening of the ear allows better hearing. We thus raised mice with tones until after ear opening into the second PNW and compared SPNs ($N = 32$) in these mice to SPNs ($N = 22$) from mice reared without sounds. These longer exposures resulted in more extensive circuit changes. SPNs in tone-exposed animals showed fewer and weaker excitatory and inhibitory inputs (Fig. 6, A and B, and fig. S4B), resulting in a decreased E/I balance index for inputs from L5/6 and within subplate (fig. S7). After sound exposure, SPNs also showed decreased map correlations, indicating increased circuit variability for both excitatory and inhibitory connections (fig. S8). Robust differences were also present when comparing animals raised under ambient versus no-sound conditions (Fig. 6, C to E). The differences to the no-sound conditions tended to be larger in the ambient versus tone-reared conditions. Together, these results show that early exposure to sound stimuli can alter cortical circuits and that the circuit changes after sound exposure are opposite from those observed in TMC1/2-DKO mice.

So far, our results have shown that early sensory manipulations resulted in circuit changes in subplate. We next asked whether these

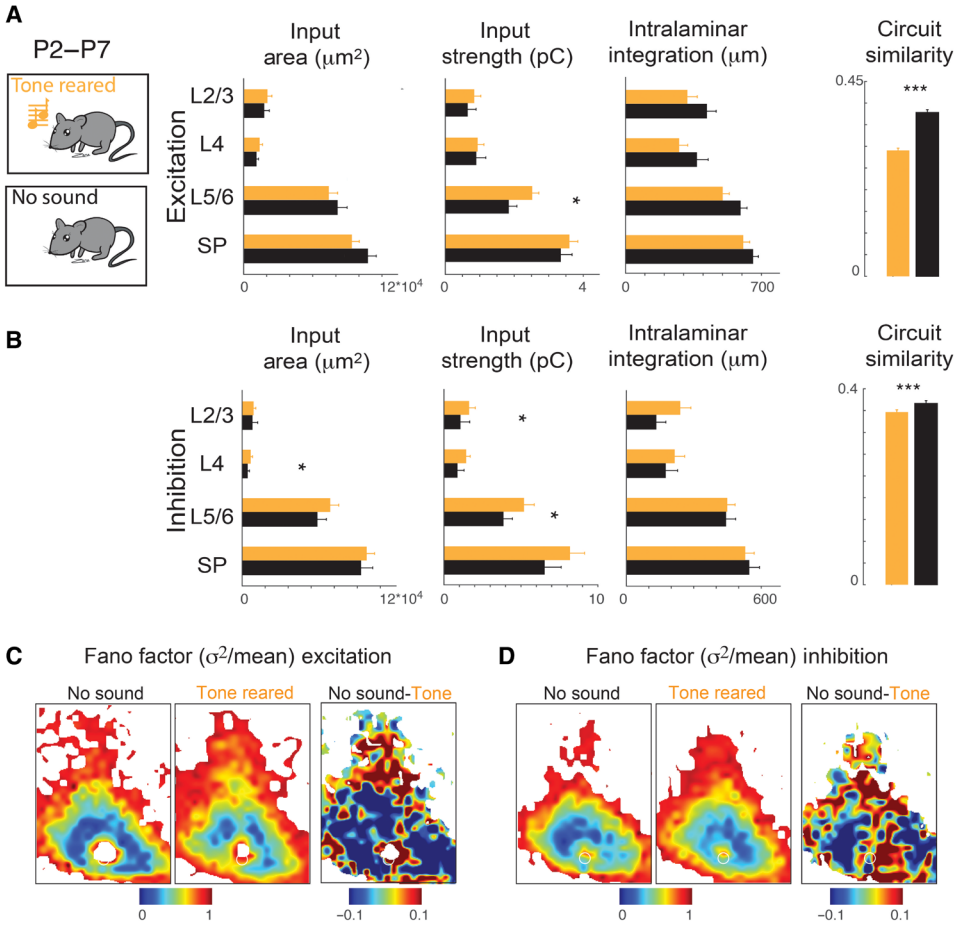

Fig. 4. Early tone exposure alters circuits to SPNs at end of first PNW. (**A**) Animals were tone-reared from P2 until end of first PNW (P6 to P9). Total source area, mean charge of eEPSCs, integration width of excitatory projections along the rostro-caudal axis, and correlation between excitatory input maps; see fig. S10. (**B**) Same as (A) but for inhibitory inputs. (**C** and **D**) Fano factor of excitatory and inhibitory maps shows increases in variability. See fig. S10 and tables S3 and S4.

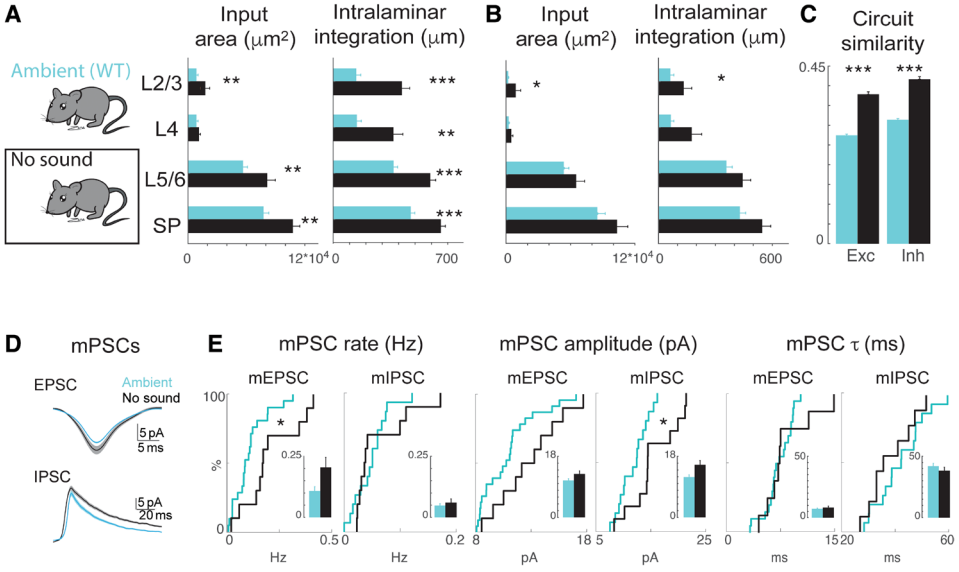

Fig. 5. Early ambient sound exposure alters circuits to SPNs at end of first PNW. (**A** and **B**) Comparison of source area, mean charge, and integration width of projections along the rostro-caudal axis between ambient-raised control mice (from Fig. 2) and no-sound mice for excitatory (A) and inhibitory (B) connections. See fig. S11. (**C**) Correlations are increased in SPNs from no-sound animals. (**D**) mEPSC and mIPSC traces in SPNs from ambient and no-sound animals. Solid lines present the mean mPSC, and shadows present SEM. (**E**) CDFs show mPSC rate, amplitude, and decay time constants; bar graph inserts show means. For all plots, *$P < 0.05$, **$P < 0.01$, and ***$P < 0.001$; see tables S5 and S6.

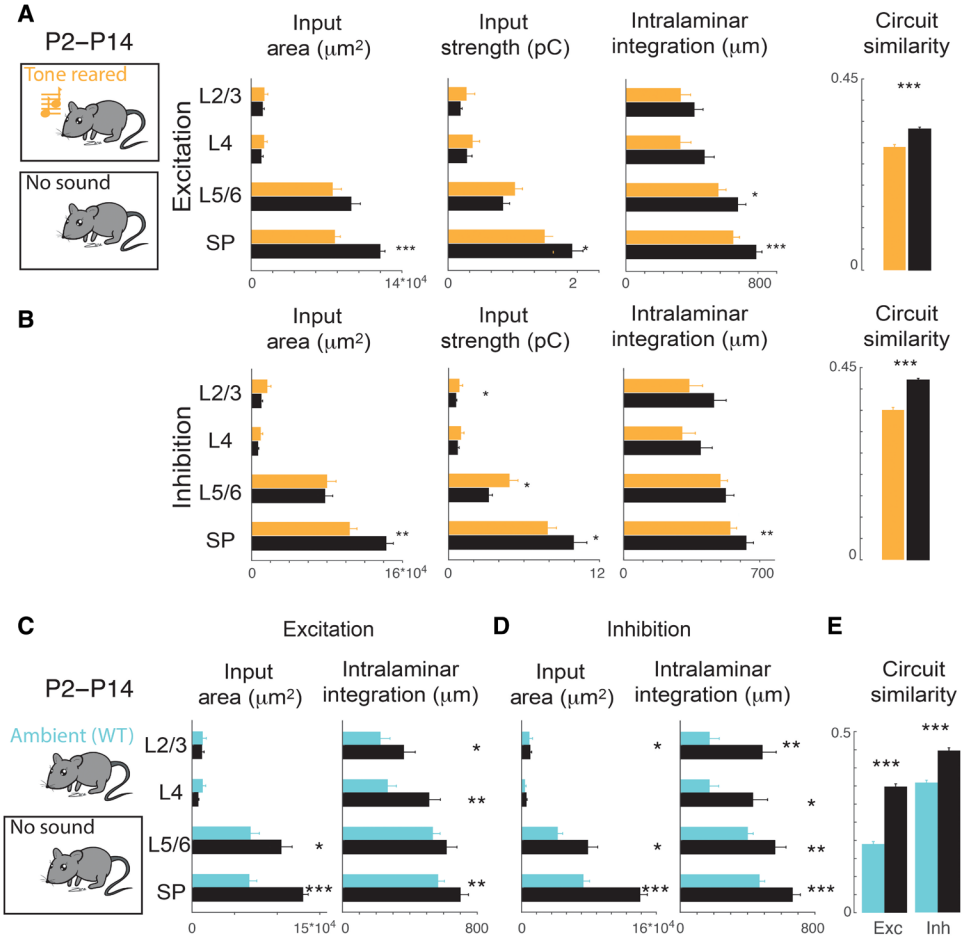

Fig. 6. Effects of tone or ambient sound exposure on SPNs are larger in second PNW. (**A**) Animals were tone-reared from P2 until end of second PNW (P10 to P16). Total source area, mean charge of eEPSCs, integration width of excitatory projections along the rostro-caudal axis, and correlation between excitatory input maps. (**B**) Same as (A) but for inhibitory inputs. See fig. S12. (**C** to **E**) Same as (A) and (B) but for comparison with ambient sound conditions. For all plots, $^{*}P < 0.05$, $^{**}P < 0.01$, and $^{***}P < 0.001$; see tables S7 to S10.

circuit changes were reflected in in vivo responses. We thus performed in vivo widefield imaging in awake mice consequent to early sound exposure (n = 6) or no-sound condition (n = 5; Fig. 7A). Compared to the no-sound conditions, animals raised with ambient sounds or with tonal stimuli showed increased spontaneous activity as indicated by smaller inter-event intervals (Fig. 7A). However, L-events were larger in these animals (Fig. 7, B and C), consistent with increased excitatory connections (Figs. 4 and 5). Because we observe a lower spatial connectivity to SPN in mice raised with ambient sounds or with tonal stimuli than in mice raised in silence, we next analyzed the correlation of activity across regions of interest (ROIs) tiling the cortical space. We find that correlations in tone- and ambient sound–exposed animals trended lower than those in the no-sound condition (Fig. 7D). Similarly, imaging in TMC1/2-DKO pups showed a higher spatial correlation of spontaneous events, indicating temporally more sparse but globally more correlated cortical activity (fig. S13). The increased correlation of cortical activity is consistent with increased cortical circuits. Together, these results indicate that early exposure to sounds causes refinement of connections to SPNs and spatially decorrelates cortical spontaneous activity, while lack of sensory input causes subplate hyperconnectivity and increased correlated activity.

DISCUSSION

The onset of the classic critical period in L4 coincides with the maturation of TC connections to L4. We delineate an earlier developmental phase during which thalamus innervates subplate. During this time, the thalamic innervation to L4 is immature, but we show that peripheral activity can bidirectionally influence circuits impinging on cortical SPNs. Thus, SPNs are the earliest substrate for experience-dependent cortical plasticity, and cortical plasticity occurs sequentially starting with the earliest maturing cortical neurons. Because previous studies on the influence of experience on cortical circuits started manipulations at a later time point, our results here suggest a reinterpretation of those studies as those animals already had previous sensory experience, which may have already shaped cortical circuits. In particular, because we observe differences between mice placed in a quiet sound chamber and mice exposed to ambient animal colony sounds, this suggests that external sounds can shape ACtx circuits at young ages and potentially bias plasticity at later ages.

Hyperconnectivity of SPNs in deaf mice is consistent with a homeostatic adjustment to decreased sound-induced activity. ACtx in both ferrets and mice show sound-evoked responses before ear opening (*27*, *32*); thus, early peripheral activity, which encompasses

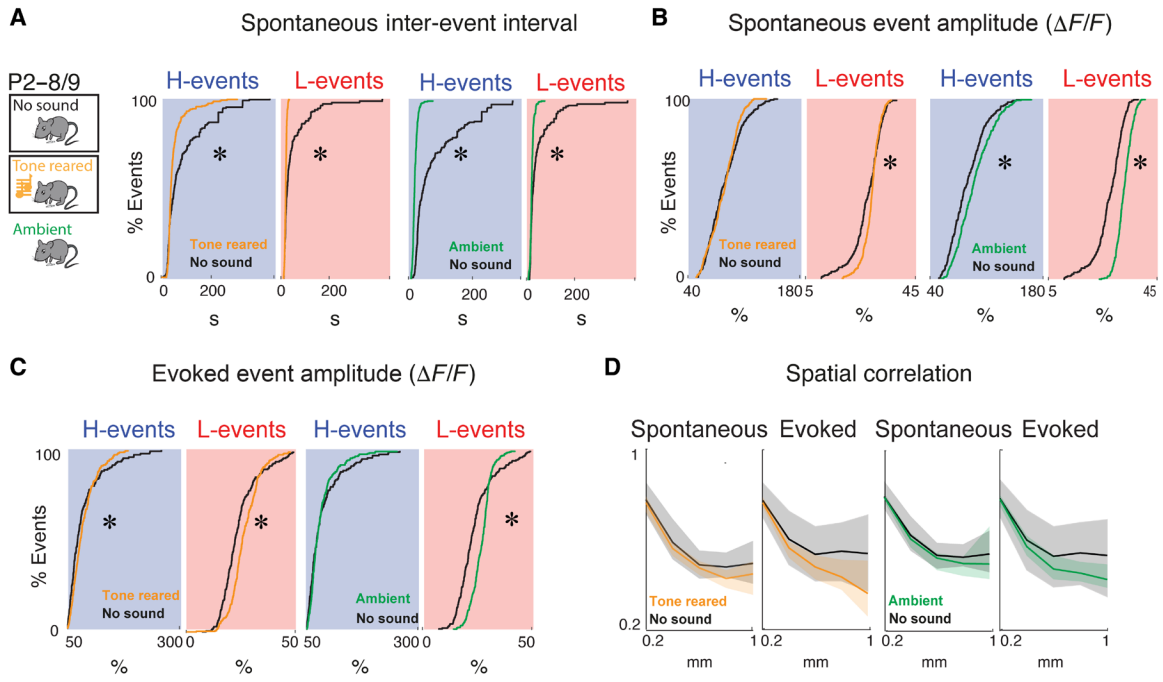

Fig. 7. Effects of early tone exposure on cortical network activity. (**A**) Inter-event interval of spontaneous L- and H-events in tone-reared (H-event median: 35.1 s, L-event median: 20.1 s) and ambient sound–experienced (H-event median: 18.7 s, L-event median: 20.6 s) mice are lower than those reared in silence (H-event median: 41.6 s, L-event median: 23.2 s; $P < 0.001$ for both). (**B**) Peak amplitude of spontaneous L-events is higher in tone-reared (median: 29.2%) and ambient sound–experienced (median: 32.7%) mice than in mice reared in silence (median: 28.2%; $P < 0.001$ for both). (**C**) Peak amplitude of evoked L-events is higher in tone-reared (median: 26%) and ambient sound–experienced (median: 27.5%) mice than in mice reared in silence (median: 22.3%; $P < 0.001$ for both). (**D**) Spatial correlation of spontaneous and sound-evoked activity is similar.

both sensorily evoked and spontaneous activity, can sculpt the nascent central circuits. While TMC1/2-DKO and tone rearing showed opposite effects, tone rearing resulted in more modest circuit changes. This is likely due to our inability to control self-generated sounds (e.g., vocalizations), movement, and the attenuation of external sounds by the closed ear. While both tones and ambient sounds alter SPN circuits, the effects of ambient sound might be larger possibly due to a broader spectral content. Together, we find that changing the ambient sound environment affects SPNs at the earliest times examined. Thus, our results show that cortical circuits can be altered by peripheral sensory stimuli before the traditional critical period. Prenatal spontaneous thalamic activity sculpts the organization of S1 barrel cortex, and this spontaneous activity can activate SPNs (*41*) and possibly also change SPN circuits. Because whisker removal can alter SPN morphology (*42*), we speculate that altered thalamic activity likely also alters SPN circuits and that such changes might underlie the TC patterning changes seen (*41*).

We here study how peripheral auditory activity shapes ACtx. SPNs are present in all sensory areas, and both the visual and the somatosensory system show early spontaneous or sensorily evoked activity, e.g., driven by vision through closed eyelids or self-generated movements (*43*–*46*). We thus speculate that alterations of these early activity patterns will also affect SPNs in the respective cortices. Moreover, in early development, there is a high amount of cross-talk between sensory systems (*47*), leading us to speculate that sensory effects could be widespread.

Our results suggest that, at early ages, sensorily driven activity can interact with peripherally generated spontaneous activity and cause cortical circuit changes. We find that auditory deprivations lead to decreased cortical activity and hyperconnectivity in SPNs. We speculate that human infants born with hearing loss might also show such circuit changes and that treatments for hearing loss such as cochlear implants have to take these altered circuits into account.

We find that SPN circuits differ between mice raised in the colony and those raised in silence chambers. The animal colony contains steady-state sounds (e.g., air conditioning) as well as transient sounds such as door opening and closing (*39*). Our work suggests that such external sounds are sufficient to sculpt cortical circuits and that especially transient and rare sounds might be able to drive immature circuits that show synaptic depression (*27*). Moreover, given that rodent pups vocalize, we speculate that self-vocalizations may be able to drive auditory cortical activity and contribute to auditory development, reminiscent of the role of in ovo vocalizations in ducklings (*48*, *49*).

We show that SPNs are the earliest cortical circuits to be altered by peripheral activity and that ambient sounds are sufficient to cause changes even before the ears open. Because newborn infants show a preference for maternal voices, we speculate that in utero plasticity driven by the maternal voice (*50*–*54*) might occur in SPNs. Our results identify SPNs as the earliest cortical substrate for experience-dependent development and suggest that cortical experience-dependent plasticity is a sequential process starting with the earliest-generated neurons.

MATERIALS AND METHODS

Animals

All procedures are approved by the University of Maryland College Park Institutional Animal Care and Use Committee. Experiments were performed in male and female mice raised in 12-hour light/12-hour dark conditions. Experiments were performed in TMC1/2 KO (*35*, *55*),

C57Bl/6, and Thy1-GCaMP6s mice (JAX strains #000664 and #024275). Founders for our TMC1/2 breeding colony were provided by A. Griffith (National Institute on Deafness and Other Communication Disorders). Average ambient sound levels in our colony are <45 dB (*40*) and <30 to 40 dB at >1 kHz.

In vivo imaging

Widefield imaging was performed as previously described (*32*, *33*). In vivo widefield imaging was performed on unanesthetized male and female Thy1-GCaMP6s transgenic mice at P8 to P9 (n = 6 pups) and P13 to P15 (n = 5 pups). Mice were bred in-house, and no more than two littermates were assigned to the same age group. Acute surgeries were performed, and pups were imaged the same day. A pup with a visible milk band was separated from the cage. It was initially anesthetized with 4% inhaled isoflurane (Fluriso, VetOne), which was later reduced to 2 to 3% for stable maintenance. A heating block was used to maintain body temperature near 37°C. The scalp fur was trimmed using scissors. Depth of anesthesia was monitored every 5 min by observing respiratory pattern and toe-pinch reflex of the pup.

The skull overlying the left ACtx was exposed, and a three-dimensionally printed stainless steel headplate was affixed with cyanoacrylate glue. Dental cement (C&B-Metabond) was applied on the outer perimeter of the headplate to secure it to the skull. The intact and exposed skull was cleaned by applying optical clearing agents (10% collagenase solution followed by 80% glycerol solution) (*56*). Meloxicam (0.5 ml) was injected subcutaneously. The pup was wrapped in a gauze, placed within a plastic box in a warm water bath for at least 30 min for recovery.

Once recovered, the pup was head restrained, placed on a far-infrared heating pad (Kent Scientific), and transferred to a soundproof recording chamber. In vivo imaging was performed through the skull. The detailed description of widefield imaging has been provided elsewhere (*57*, *58*). Briefly, blue light-emitting diode (LED) light (470-nm; Thorlabs) was used for excitation of GCaMP6s fluorescence. Emitted light was collected using a tandem lens combination setup (*57*, *59*). Images were captured using ThorCam software (Thorlabs) that controls a Thorlabs DCC3240M CMOS (complementary metal-oxide semiconductor) camera. An image of the surface vasculature was acquired. Then, the focal plane was advanced to a depth of ~200 to 500 μm below the brain surface, where the rest of widefield imaging was performed at a rate of 4 Hz and 640 × 512 pixels with a 100-ms exposure time.

Spontaneous cortical activity was first recorded for 10 min during which no sound was played. Next, to investigate sound-evoked cortical activity, pure tones of frequencies 4, 8, 16, and 32 kHz were generated using custom software in MATLAB and played randomly from a free field speaker at an intensity of 80-dB sound pressure level. Each frequency was randomly repeated 10 to 12 times with an intertrial interval of 30 s. Each trial consisted of 2-s prestimulus silence, 1-s tone presentation, and 5-s post-stimulus silence.

If the pup exhibited any signs of distress, the experiment was terminated immediately. At the end of the experiment, the pup was euthanized.

Widefield imaging data were analyzed using custom routines in MATLAB (MathWorks). Dimensionality reduction was used to perform automatic image segmentation so that pixels with strong temporal correlations across the image were grouped together into single components. An autoencoder neural network was used to perform the dimensionality reduction (*33*). For each ROI, we calculated the amplitude and frequency of spontaneous events and events during sound stimulation.

For each trial, the response amplitude ($\Delta F/F$) as a function of time for each ROI was determined using the following formula, $(F - F_0)/F_0$, where F corresponds to the time-varying fluorescence at a given ROI. F_0 was the baseline fluorescence. For spontaneous trials, we estimated F_0 by finding the first percentile of fluorescence values in sliding windows, the centers of which are equally spaced across the whole trial (window size = 300 frames), and using linear interpolation methods (MATLAB built-in function regress) across all windows. For tone-evoked responses, F_0 is the first percentile of fluorescence within a 2-s window" before tone onset.

For each ROI, we calculated the averaged $\Delta F/F$ within a 2-s window before and after tone onset for each trial and evaluate active ROIs with a paired sample t test comparison between the two averaged $\Delta F/F$ across all the repeats for each frequency (Fig. 1). Active ROIs are the ones that show significant difference ($P < 0.05$) at least for one sound frequency. To visualize active ROIs, we plotted the active ROIs with pseudocolor (Fig. 1C).

To identify L- and H-events, we first detected peaks in the fluorescence responses in MATLAB using the built-in peak detection function (findpeaks) with minimum peak prominence = 0.1 and minimum peak distance = 1 frame. To separate L- and H-events, we used a threshold of 50% $\Delta F/F$ (Fig. 1E). The response amplitudes of L/H-events across all the repeats over spontaneous trials or in a period of 2 s after tone onset for each ROI were compared between populations with Student's t test or rank sum test based on Lilliefors test for normality (Fig. 1). Varying the threshold for detecting L- and H-events by ±10% did not affect our conclusions.

In vitro physiology

In vitro recordings from brain slices were performed as previously described (*12*, *15*, *60*). Mice were deeply anesthetized with isoflurane (Halocarbon). A block of brain containing A1 and the medial geniculate nucleus is removed, and TC slices (500 μm thick) are cut on a vibrating microtome (Leica) in ice-cold artificial cerebrospinal fluid (ACSF) containing 130 mM NaCl, 3 mM KCl, 1.25 mM KH_2PO_4, 20 mM $NaHCO_3$, 10 mM glucose, 1.3 mM $MgSO_4$, and 2.5 mM $CaCl_2$ (pH 7.35 to 7.4, in 95% O_2–5% CO_2). For A1 slices, the cutting angle is ~15° from the horizontal plane (lateral raised) (*15*, *60*). Slices are incubated for 1 hour in ACSF at 30°C and then kept at room temperature. For recording, slices are held in a chamber on a fixed-stage microscope (Olympus BX51) and superfused (2 to 4 ml/min) with high-Mg^{2+} ACSF recording solution at room temperature to reduce spontaneous activity in the slice. The recording solution contained 124 mM NaCl, 5 mM KCl, 1.23 mM NaH_2PO_4, 26 mM $NaHCO_3$, 10 mM glucose, 4 mM $MgCl_2$, and 4 mM $CaCl_2$. The location of the recording site in A1 was identified by landmarks (*15*, *60*). mPSC recordings were made in the presence of 1 μM tetrodotoxin in the regular ACSF.

Whole-cell recordings are performed with a patch clamp amplifier (MultiClamp 700B, Axon Instruments) using pipettes with input resistance of 4 to 9 megohms. Data acquisition is performed by National Instruments Data acquisition boards and custom software (Ephus) (*61*) written in MATLAB (MathWorks). Voltages were corrected for an estimated junction potential of 10 mV. Electrodes are filled with 115 mM cesium methanesulfonate ($CsCH_3SO_3$), 5 mM NaF, 10 mM EGTA, 10 mM Hepes, 15 mM CsCl, 3.5 mM Mg adenosine

triphosphate (ATP), and 3 mM QX-314 (pH 7.25, 300 mOsm). Biocytin or Neurobiotin (0.5%) is added to the electrode solution as needed. Series resistances were typically 20 to 25 megohms. Photostimulation: 0.5 to 1 mM caged glutamate [*N*-(6-nitro-7-coumarylmethyl)-L-glutamate] (*62*, *63*) is added to the ACSF. Without ultraviolet (UV) light, this compound has no effect on neuronal activity (*62*). UV laser light (500 mW, 355 nm, 1-ms pulses, and 100-kHz repetition rate; DPSS Laser Inc., Santa Clara, CA) is split by a 33% beam splitter (CVI Melles Griot), attenuated by a Pockels cell (Conoptics), gated with a laser shutter (NM Laser), and coupled into a microscope via scan mirrors (Cambridge Technology) and a dichroic mirror. The laser beam enters the slice axially through the objective (Olympus 10×, 0.3 numerical aperture/water) and has a diameter of <20 μm. Laser power at the sample is <25 mW. We typically stimulated up to 30 × 35 sites spaced 40 μm apart, enabling us to probe areas of 1 mm^2; such dense sampling reduces the influence of potential spontaneous events. Stimuli are applied at 0.5 to 1 Hz. Analysis was performed as described previously (*12*, *32*, *57*) with custom software written in MATLAB. Activation profiles of neurons were produced by recording in cell-attached mode while mapping the same region and recording action potentials. To detect monosynaptically evoked PSCs, we detected PSCs with onsets in an approximately 50-ms window after the stimulation. This window was chosen on the basis of the observed spiking latency under our recording conditions (*12*, *13*, *32*).

Our recordings are performed at room temperature and in high-Mg^{2+} solution to reduce the probability of multisynaptic inputs. Our analysis was done as in our previous studies (*12*, *32*, *57*). We measured both peak amplitude and transferred charge (integrating the PSC). While the transferred charge might include contributions from multiple events, our previous studies showed a strong correlation between these measures (*12*, *13*). Traces containing a short-latency (<8 ms) "direct" response were discarded from the analysis (black patches in color-coded maps), as were traces that contained longer latency inward currents of long duration (>50 ms). These currents could sometimes be seen in locations surrounding (<100 μm) areas that gave a direct response. Occasionally, some of the direct responses contained synaptic evoked responses that we did not separate out, leading to an underestimation of local short-range connections. Cells that did not show any large (>100 pA) direct responses were excluded from the analysis, as these could reflect astrocytes or migrating neurons. It is likely that the observed PSCs at each stimulus location represent the activity of multiple presynaptic cells.

Stimulus locations that showed PSC were deemed connected, and we derived binary connection maps. We aligned connection maps for SPNs in the population and averaged connection maps to derive a spatial connection probability map. In these maps, the value at each stimulus location indicates the fraction of SPNs that received input from these stimulus locations. Layer boundaries were determined from the infrared pictures. We derived laminar measures. We calculated the input area for each layer as a measure reflecting the number of presynaptic neurons in each layer projecting to the cell under study. Input area is calculated as the area within each layer that gave rise to PSCs. Mean charge is the average charge of PSCs from each stimulus location in each layer. Intralaminar integration distance is the extent in the rostro-caudal direction that encompasses connected stimulus locations in each layer. Because the tonotopic map is largely in the rostro-caudal axis, the intralaminar integration distance reflects integration across the tonotopic axis. While the input area and intralaminar integration are related, the input area will also show changes along the columnar (pia-ventricle) axis if more or less cells within a tonotopic place are recruited, e.g., only L5 cells versus L5 and L6 cells. We calculated the E/I balance index in each layer for measures of input area and strength as $(E - I)/(E + I)$; thus, $(Area_E - Area_I)/(Area_E + Area_I)$, resulting in a number that varied between −1 and 1, with 1 indicating dominant excitation and −1 indicating dominant inhibition. Because a measurement of E is not possible close to the soma due to direct responses, we excluded the direct area from both the E and I maps. Thus, this E/I measure does not account for the contribution for cells from closeby locations but does allow analysis of the E/I balance of inputs arising from different layers. The E/I balance for mini PSCs was calculated as the integrated charge over the recorded mEPSCs and mIPSCs within the 10-min recording interval.

Spatial connection probability maps show the average connection pattern in each group. To visualize the diversity of connection patterns over the population of neurons in each group, we calculated Fano factor maps. For each responsive spatial location, we calculated the Fano factor of the PSC evoked from this stimulation site across population of neurons as σ^2/μ. We then plotted maps of the Fano factor. We did not compute a Fano factor in areas where the connection probability is <10% and indicated those with white in the maps. To compare the large-scale connectivity between cells in each group, we calculated the spatial correlation of the binary connection maps in each group by calculating the pairwise cross-correlations (*32*).

Tone rearing

Mice were raised in a cage inside an enclosed sound attenuating chamber, providing >20-dB attenuation at >1 kHz (*38*, *64*). The whole litter was transferred into the chamber at P2. Care was taken to not disturb the cage during the first 48 hours after birth. The light cycle was maintained at 12-hour light/12-hour dark (*38*). Pure tones of frequencies 4, 8, 16, and 32 kHz and 1-s duration were played throughout the day randomly with a 30-s interstimulus interval with an intensity at the speaker of 80 dB (<20 dB above threshold) (*65*). The speaker was located inside the cage (*38*). The control litters were placed in the sound attenuating chambers and treated in the same way, except no tones were played (no-sound condition). Animals were checked for health twice daily.

Intracerebroventricular injection of AAV-GCaMP6s virus

Unilateral intracerebroventricular injection of AAV.CamKII.GCaMP6s.WPRE.SV40 virus (Addgene # 107790-AAV9) was performed at P2 in TMC1/2-DKO ($n = 2$) and C57BL/6J ($n = 2$) pups. Aliquots of the virus were removed from −80°C and thawed on ice before injection. A metal plate was placed on ice to cool. A pup with a visible milk band was isolated from the litter, lightly wrapped in a dry task wipe, and placed on the cold metal plate to induce hypothermia anesthesia. Anesthesia was confirmed by tail pinch and lack of movement of the pup. A 10-μl Hamilton syringe with a 32-gauge needle was loaded with the virus. The injection site was marked at 1 mm lateral to the sagittal suture (left hemisphere), halfway between lambda and bregma. The landmarks were visible through the skin at these ages. The pup's head was held steadily with fingers, and the needle was inserted perpendicular to the surface at a depth of ~3 mm. A little decrease in resistance confirmed the needle's penetration into the lateral ventricle. Virus (1.5 to 2 μl) was injected over 60 s, and then the needle was slowly withdrawn. The injection site was wiped

with alcohol pad, and the pup was transferred to a heating pad to recover. Once it started showing movements, the other littermates were also placed on the heating pad. After 10 to 15 min, the litter was returned to their home cage.

Bilateral cochlear ablation surgery

Bilateral cochlear ablation surgery was performed in five pups expressing GCaMP6s from three litters at P6 to P7 following established protocols (*66*). A pup with a visible milk band was isolated from the litter and anesthetized with 3% isoflurane in the induction chamber. It was then moved to a heating pad, and anesthesia was maintained at 3% using a nose cone for the entire duration of the surgery. The pup was placed on its side, and 0.1 ml of lidocaine was applied in the cheek along an imaginary line ventral to the ear and caudal to the mouth. Using microscissors, a small incision was made slightly below the imaginary line. Fine forceps and scissors were used carefully to clear tissues and fat to approach the bulla bone. A major blood vessel, dorsal and posterior to the bulla bone, and the facial nerve along the rostral-caudal axis were used as prominent landmarks. The C-shaped end of the bulla bone was identified. A 27-gauge needle was then used to break through the bone, and fine forceps were used to peel it away from the posterior to the anterior end. The basal turn of the cochlea rests beneath the bone. Fine forceps and a 27-gauge vacuum needle were used to pull out the gelatinous mesenchyme from the middle ear, exposing the bony covering of the cochlea. The bone was then broken through using a 27-gauge needle, and the entire cochlea was aspirated. The damage was packed with surgical foam soaked in sterile saline, and the incision was closed with surgical sutures. The same process was repeated on the other ear. At the end of the surgery, the pup was injected with 0.1 ml of meloxicam (subcutaneously) and placed on a heating pad for recovery. After recovery (~30 min), the pup was returned to its home cage. The health of the pup was monitored twice daily after surgery until it was used for in vivo imaging.

Statistics

Results are plotted as means ± SD, unless otherwise indicated. Populations in LSPS results are compared with Student's *t* test or rank sum test (based on Lilliefors test for normality).

SUPPLEMENTARY MATERIALS

Supplementary material for this article is available at http://advances.sciencemag.org/cgi/content/full/7/7/eabc9155/DC1

View/request a protocol for this paper from *Bio-protocol*.

REFERENCES AND NOTES

1. T. R. Barkat, D. B. Polley, T. K. Hensch, A critical period for auditory thalamocortical connectivity. *Nat. Neurosci.* **14**, 1189–1194 (2011).
2. J. S. Espinosa, M. P. Stryker, Development and plasticity of the primary visual cortex. *Neuron* **75**, 230–249 (2012).
3. R. S. Erzurumlu, P. Gaspar, Development and critical period plasticity of the barrel cortex. *Eur. J. Neurosci.* **35**, 1540–1553 (2012).
4. D. H. Sanes, S. Bao, Tuning up the developing auditory CNS. *Curr. Opin. Neurobiol.* **19**, 188–199 (2009).
5. L. I. Zhang, S. Bao, M. M. Merzenich, Persistent and specific influences of early acoustic environments on primary auditory cortex. *Nat. Neurosci.* **4**, 1123–1130 (2001).
6. J. A. Wen, A. L. Barth, Input-specific critical periods for experience-dependent plasticity in layer 2/3 pyramidal neurons. *J. Neurosci.* **31**, 4456–4465 (2011).
7. M. Hubener, T. Bonhoeffer, Neuronal plasticity: Beyond the critical period. *Cell* **159**, 727–737 (2014).
8. P. O. Kanold, H. J. Luhmann, The subplate and early cortical circuits. *Annu. Rev. Neurosci.* **33**, 23–48 (2010).
9. Z. Molnár, H. J. Luhmann, P. O. Kanold, Transient cortical circuits match spontaneous and sensory-driven activity during development. *Science* **370**, eabb2153 (2020).
10. J. C. Birnholz, B. R. Benacerraf, The development of human fetal hearing. *Science* **222**, 516–518 (1983).
11. C. Porcaro, F. Zappasodi, G. Barbati, C. Salustri, V. Pizzella, P. M. Rossini, F. Tecchio, Fetal auditory responses to external sounds and mother's heart beat: Detection improved by Independent Component Analysis. *Brain Res.* **1101**, 51–58 (2006).
12. X. Meng, J. P. Y. Kao, P. O. Kanold, Differential signaling to subplate neurons by spatially specific silent synapses in developing auditory cortex. *J. Neurosci.* **34**, 8855–8864 (2014).
13. S. Viswanathan, S. Bandyopadhyay, J. P. Y. Kao, P. O. Kanold, Changing microcircuits in the subplate of the developing cortex. *J. Neurosci.* **32**, 1589–1601 (2012).
14. S. Viswanathan, A. Sheikh, L. L. Looger, P. O. Kanold, Molecularly defined subplate neurons project both to thalamocortical recipient layers and thalamus. *Cereb. Cortex* **27**, 4759–4768 (2016).
15. C. Zhao, J. P. Y. Kao, P. O. Kanold, Functional excitatory microcircuits in neonatal cortex connect thalamus and layer 4. *J. Neurosci.* **29**, 15479–15488 (2009).
16. M. B. Luskin, C. J. Shatz, Studies of the earliest generated cells of the cat's visual cortex: Cogeneration of subplate and marginal zones. *J. Neurosci.* **5**, 1062–1075 (1985).
17. J. G. Wood, S. Martin, D. J. Price, Evidence that the earliest generated cells of the murine cerebral cortex form a transient population in the subplate and marginal zone. *Brain Res.* **66**, 137–140 (1992).
18. D. J. Price, S. Aslam, L. Tasker, K. Gillies, Fates of the earliest generated cells in the developing murine neocortex. *J. Comp. Neurol.* **377**, 414–422 (1997).
19. A. Hoerder-Suabedissen, Z. Molnár, Molecular diversity of early-born subplate neurons. *Cereb. Cortex* **23**, 1473–1483 (2012).
20. R. T. Robertson, C. M. Annis, J. Baratta, S. Haraldson, J. Ingeman, G. H. Kageyama, E. Kimm, J. Yu, Do subplate neurons comprise a transient population of cells in developing neocortex of rats? *J. Comp. Neurol.* **426**, 632–650 (2000).
21. P. O. Kanold, P. Kara, R. C. Reid, C. J. Shatz, Role of subplate neurons in functional maturation of visual cortical columns. *Science* **301**, 521–525 (2003).
22. P. O. Kanold, C. J. Shatz, Subplate neurons regulate maturation of cortical inhibition and outcome of ocular dominance plasticity. *Neuron* **51**, 627–638 (2006).
23. E. A. Tolner, A. Sheikh, A. Y. Yukin, K. Kaila, P. O. Kanold, Subplate neurons promote spindle bursts and thalamocortical patterning in the neonatal rat somatosensory cortex. *J. Neurosci.* **32**, 692–702 (2012).
24. D. A. Nagode, X. Meng, D. E. Winkowski, E. Smith, H. Khan-Tareen, V. Kareddy, J. P. Y. Kao, P. O. Kanold, Abnormal development of the earliest cortical circuits in a mouse model of autism spectrum disorder. *Cell Rep.* **18**, 1100–1108 (2017).
25. A. Sheikh, X. Meng, J. Liu, A. Mikhailova, J. P. Y. Kao, P. S. McQuillen, P. O. Kanold, Neonatal hypoxia-ischemia causes functional circuit changes in subplate neurons. *Cereb. Cortex* **29**, 765–776 (2019).
26. C. Nicolini, M. Fahnestock, The valproic acid-induced rodent model of autism. *Exp. Neurol.* **299**, 217–227 (2018).
27. J. M. Wess, A. Isaiah, P. V. Watkins, P. O. Kanold, Subplate neurons are the first cortical neurons to respond to sensory stimuli. *Proc. Natl. Acad. Sci. U.S.A.* **114**, 12602–12607 (2017).
28. H. C. Wang, D. E. Bergles, Spontaneous activity in the developing auditory system. *Cell Tissue Res.* **361**, 65–75 (2015).
29. T. A. Babola, S. Li, A. Gribizis, B. J. Lee, J. B. Issa, H. C. Wang, M. C. Crair, D. E. Bergles, Homeostatic control of spontaneous activity in the developing auditory system. *Neuron* **99**, 511–524.e5 (2018).
30. A. Clause, G. Kim, M. Sonntag, C. J. C. Weisz, D. E. Vetter, R. Rubsamen, K. Kandler, The precise temporal pattern of prehearing spontaneous activity is necessary for tonotopic map refinement. *Neuron* **82**, 822–835 (2014).
31. M. Geal-Dor, S. Freeman, G. Li, H. Sohmer, Development of hearing in neonatal rats: Air and bone conducted ABR thresholds. *Hear. Res.* **69**, 236–242 (1993).
32. X. Meng, K. Solarana, Z. Bowen, J. Liu, D. A. Nagode, A. Sheikh, D. E. Winkowski, J. P. Y. Kao, P. O. Kanold, Transient subgranular hyperconnectivity to L2/3 and enhanced pairwise correlations during the critical period in the mouse auditory cortex. *Cereb. Cortex* **30**, 1914–1930 (2019).
33. J. Liu, M. R. Whiteway, A. Sheikhattar, D. A. Butts, B. Babadi, P. O. Kanold, Parallel processing of sound dynamics across mouse auditory cortex via spatially patterned thalamic inputs and distinct areal intracortical circuits. *Cell Rep.* **27**, 872–885.e7 (2019).
34. F. Siegel, J. A. Heimel, J. Peters, C. Lohmann, Peripheral and central inputs shape network dynamics in the developing visual cortex in vivo. *Curr. Biol.* **22**, 253–258 (2012).
35. B. Pan, G. S. Geleoc, Y. Asai, G. C. Horwitz, K. Kurima, K. Ishikawa, Y. Kawashima, A. J. Griffith, J. R. Holt, TMC1 and TMC2 are components of the mechanotransduction channel in hair cells of the mammalian inner ear. *Neuron* **79**, 504–515 (2013).
36. Y. Kawashima, G. S. G. Geleoc, K. Kurima, V. Labay, A. Lelli, Y. Asai, T. Makishima, D. K. Wu, C. C. Della Santina, J. R. Holt, A. J. Griffith, Mechanotransduction in mouse

inner ear hair cells requires transmembrane channel-like genes. *J. Clin. Invest.* **121**, 4796–4809 (2011).
37. C. Askew, C. Rochat, B. Pan, Y. Asai, H. Ahmed, E. Child, B. L. Schneider, P. Aebischer, J. R. Holt, Tmc gene therapy restores auditory function in deaf mice. *Sci. Transl. Med.* **7**, 295ra108 (2015).
38. N. A. Francis, K. Bohlke, P. O. Kanold, Automated behavioral experiments in mice reveal periodic cycles of task engagement within circadian rhythms. *eNeuro* **6**, ENEURO.0121-19.2019, (2019).
39. A. M. Lauer, B. J. May, Z. J. Hao, J. Watson, Analysis of environmental sound levels in modern rodent housing rooms. *Lab Anim. (NY)* **38**, 154–160 (2009).
40. E. Petrus, A. Isaiah, A. P. Jones, D. Li, H. Wang, H. K. Lee, P. O. Kanold, Crossmodal induction of thalamocortical potentiation leads to enhanced information processing in the auditory cortex. *Neuron* **81**, 664–673 (2014).
41. N. Anton-Bolanos, A. Sempere-Ferrandez, T. Guillamon-Vivancos, F. J. Martini, L. Perez-Saiz, H. Gezelius, A. Filipchuk, M. Valdeolmillos, G. Lopez-Bendito, Prenatal activity from thalamic neurons governs the emergence of functional cortical maps in mice. *Science* **364**, 987–990 (2019).
42. M. C. Pinon, A. Jethwa, E. Jacobs, A. Campagnoni, Z. Molnar, Dynamic integration of subplate neurons into the cortical barrel field circuitry during postnatal development in the Golli-tau-eGFP (GTE) mouse. *J. Physiol.* **587**, 1903–1915 (2009).
43. A. G. Blankenship, M. B. Feller, Mechanisms underlying spontaneous patterned activity in developing neural circuits. *Nat. Rev. Neurosci.* **11**, 18–29 (2010).
44. R. Khazipov, H. J. Luhmann, Early patterns of electrical activity in the developing cerebral cortex of humans and rodents. *Trends Neurosci.* **29**, 414–418 (2006).
45. K. Krug, C. J. Akerman, I. D. Thompson, Responses of neurons in neonatal cortex and thalamus to patterned visual stimulation through the naturally closed lids. *J. Neurophysiol.* **85**, 1436–1443 (2001).
46. J. C. Dooley, R. M. Glanz, G. Sokoloff, M. S. Blumberg, Self-generated whisker movements drive state-dependent sensory input to developing barrel cortex. *Curr. Biol.* **30**, 2404–2410.e4 (2020).
47. J. U. Henschke, A. M. Oelschlegel, F. Angenstein, F. W. Ohl, J. Goldschmidt, P. O. Kanold, E. Budinger, Early sensory experience influences the development of multisensory thalamocortical and intracortical connections of primary sensory cortices. *Brain Struct. Funct.* **223**, 1165–1190 (2018).
48. L. P. Dmitrieva, G. Gottlieb, Development of brainstem auditory pathway in mallard duck embryos and hatchlings. *J. Comp. Physiol. A* **171**, 665–671 (1992).
49. G. Gottlieb, *Development of Species Identification in Birds: An Inquiry into the Prenatal Determinants of Perception* (University of Chicago Press, ed. 1, 1971), p. 176.
50. A. J. DeCasper, W. P. Fifer, Of human bonding: Newborns prefer their mothers' voices. *Science* **208**, 1174–1176 (1980).
51. J. Mehler, P. Jusczyk, G. Lambertz, N. Halsted, J. Bertoncini, C. Amiel-Tison, A precursor of language acquisition in young infants. *Cognition* **29**, 143–178 (1988).
52. K. M. Voegtline, K. A. Costigan, H. A. Pater, J. A. DiPietro, Near-term fetal response to maternal spoken voice. *Infant Behav. Dev.* **36**, 526–533 (2013).
53. G. A. Ferrari, Y. Nicolini, E. Demuru, C. Tosato, M. Hussain, E. Scesa, L. Romei, M. Boerci, E. Iappini, G. D. R. Prati, E. Palagi, P. F. Ferrari, Ultrasonographic investigation of human fetus responses to maternal communicative and non-communicative stimuli. *Front. Psychol.* **7**, 354 (2016).
54. B. Mampe, A. D. Friederici, A. Christophe, K. Wermke, Newborns' cry melody is shaped by their native language. *Curr. Biol.* **19**, 1994–1997 (2009).
55. K. Kurima, L. M. Peters, Y. Yang, S. Riazuddin, Z. M. Ahmed, S. Naz, D. Arnaud, S. Drury, J. Mo, T. Makishima, M. Ghosh, P. S. N. Menon, D. Deshmukh, C. Oddoux, H. Ostrer, S. Khan, S. Riazuddin, P. L. Deininger, L. L. Hampton, S. L. Sullivan, J. F. Battey Jr., B. J. B. Keats, E. R. Wilcox, T. B. Friedman, A. J. Griffith, Dominant and recessive deafness caused by mutations of a novel gene, TMC1, required for cochlear hair-cell function. *Nat. Genet.* **30**, 277–284 (2002).
56. Y. J. Zhao, T. T. Yu, C. Zhang, Z. Li, Q. M. Luo, T. H. Xu, D. Zhu, Skull optical clearing window for in vivo imaging of the mouse cortex at synaptic resolution. *Light Sci. Appl.* **7**, 17153 (2018).
57. X. Meng, D. E. Winkowski, J. P. Y. Kao, P. O. Kanold, Sublaminar subdivision of mouse auditory cortex layer 2/3 based on functional translaminar connections. *J. Neurosci.* **37**, 10200–10214 (2017).
58. N. A. Francis, D. E. Winkowski, A. Sheikhattar, K. Armengol, B. Babadi, P. O. Kanold, Small networks encode decision-making in primary auditory cortex. *Neuron* **97**, 885–897.e6 (2018).
59. E. H. Ratzlaff, A. Grinvald, A tandem-lens epifluorescence macroscope: Hundred-fold brightness advantage for wide-field imaging. *J. Neurosci. Methods* **36**, 127–137 (1991).
60. S. J. Cruikshank, H. J. Rose, R. Metherate, Auditory thalamocortical synaptic transmission in vitro. *J. Neurophysiol.* **87**, 361–384 (2002).
61. B. A. Suter, T. O'Connor, V. Iyer, L. T. Petreanu, B. M. Hooks, T. Kiritani, K. Svoboda, G. M. G. Shepherd, Ephus: Multipurpose data acquisition software for neuroscience experiments. *Front. Neural Circuits* **4**, 100 (2010).
62. J. P. Y. Kao, Caged molecules: Principles and practical considerations, in *Current Protocols in Neuroscience*, C. Gerfen, A. Holmes, M. Rogawski, D. Sibley, P. Skolnick, S. Wray, Eds. (Wiley, 2006), vol. Unit 6.20.
63. S. Muralidharan, N. D. A. Dirda, E. J. Katz, C.-M. Tang, S. Bandyopadhyay, P. O. Kanold, J. P. Y. Kao, Ncm, a photolabile group for preparation of caged molecules: Synthesis and biological application. *PLOS ONE* **11**, e0163937 (2016).
64. N. A. Francis, P. O. Kanold, Automated operant conditioning in the mouse home cage. *Front. Neural Circuits* **11**, 10 (2017).
65. A. Shnerson, R. Pujol, Age-related changes in the C57BL/6J mouse cochlea. I. Physiological findings. *Brain Res.* **2**, 65–75 (1981).
66. S. R. Franklin, J. K. Brunso-Bechtold, C. K. Henkel, Unilateral cochlear ablation before hearing onset disrupts the maintenance of dorsal nucleus of the lateral lemniscus projection patterns in the rat inferior colliculus. *Neuroscience* **143**, 105–115 (2006).

Acknowledgments: We thank A. Griffith (NIDCD) for the TMC1/2-DKO mice and K. Bohlke, K. Shilling-Scrivo, and B. Xue for technical and surgical help. **Funding:** This study was supported by NIH R01DC009607 (P.O.K.) and NIH R01GM056481 (J.P.Y.K.). **Author contributions:** P.O.K. designed and supervised the research. X.M. performed the electrophysiological in vitro LSPS experiments and analyzed the LSPS data. D.M. performed the in vivo imaging. X.M. and D.M. analyzed the in vivo imaging data. P.O.K. wrote the manuscript. All authors edited the manuscript. J.P.Y.K. contributed the reagents. **Competing interests:** The authors declare that they have no competing interests. **Data and materials availability:** All data needed to evaluate the conclusions in the paper are present in the paper and/or the Supplementary Materials. Additional data related to this paper may be requested from the authors.

Submitted 20 May 2020
Accepted 28 December 2020
Published 12 February 2021
10.1126/sciadv.abc9155

Citation: X. Meng, D. Mukherjee, J. P. Y. Kao, P. O. Kanold, Early peripheral activity alters nascent subplate circuits in the auditory cortex. *Sci. Adv.* **7**, eabc9155 (2021).